

ANALYZING MODEL MISSPECIFICATION IN QUANTITATIVE MRI: APPLICATION TO PERFUSION ASL

Jiachen Wang[†], Jonathan I. Tamir^{*}, Adam Bush[†]

[†] The University of Texas, Austin, BME ^{*} The University of Texas, Austin, ECE

ABSTRACT

Quantitative MRI (qMRI) involves parameter estimation governed by an explicit signal model. However, these models are often confounded and difficult to validate *in vivo*. A model is misspecified when the assumed signal model differs from the true data-generating process. Under misspecification, the variance of any unbiased estimator is lower-bounded by the misspecified Cramér–Rao bound (MCRB), and maximum-likelihood estimates (MLE) may exhibit bias and inconsistency. Based on these principles, we assess misspecification in qMRI using two tests: (i) examining whether empirical MCRB asymptotically approaches the CRB as repeated measurements increase; (ii) comparing MLE estimates from two equal-sized subsets and evaluating whether their empirical variance aligns with theoretical CRB predictions. We demonstrate the framework using arterial spin labeling (ASL) as an illustrative example. Our result shows the commonly used ASL signal model appears to be specified in the brain and moderately misspecified in the kidney. The proposed framework offers a general, theoretically grounded approach for assessing model validity in quantitative MRI.

Index Terms— Quantitative Magnetic Resonance Imaging (qMRI), Model Misspecification, Misspecified Cramér–Rao Bound (MCRB), Arterial Spin Labeling (ASL), Statistical Estimation

1. INTRODUCTION

Quantitative MRI (qMRI) relies on a biophysical model that links the acquired signal to physiological parameters. Therefore, accurate parameter estimation depends on the validity of the signal models. Ideally, models are validated using an independent clinical standard test, which may be unavailable in some applications. In statistical learning, a model is said to be *misspecified* when the assumed signal-generation process differs from the true data-generating distribution [1]. Model misspecification can induce systematic bias and increased vari-

ance in parameter estimates, which in turn undermines the reliability and interpretability of qMRI.

Model validity in qMRI has been explored through two general directions. First, goodness-of-fit-based metrics evaluate how well the model explains the data using residual analysis, split-data reproducibility, or sensitivity of estimates to fixed parameters [2]. These methods can reveal poor fits but do not provide a statistical measure of how model mismatch affects estimator variance or consistency. Second, model-refinement approaches introduce extended or multi-compartment biophysical models to improve physiological plausibility [3]. While these approaches reduce mismatch, they do not evaluate how misspecified the original model is, and whether the proposed model is truly better specified.

A complementary statistical framework for assessing misspecification is the misspecified Cramér–Rao bound (MCRB) [4, 5], which generalizes the conventional Cramér–Rao bound (CRB) to account for potential model mismatch. While the MCRB has been used in economics [6] and wireless communications [7], it has not been applied as a tool in qMRI. Our work fills this gap by introducing a practical MCRB-based framework that provides a quantitative misspecification metric and corresponding voxelwise maps.

When a model is misspecified, two consequences follow: (i) the minimum achievable variance of an unbiased estimator is limited by the MCRB, which provides a strictly looser bound than the conventional CRB [5]; (ii) under maximum-likelihood estimation (MLE), parameter estimates can exhibit data-dependent biases and inconsistency [4]. Misspecification may be due either to incorrect fixed parameters of the model or to an incorrect parametric model itself [1].

Guided by the theory above, we propose two tests for assessing misspecification. First, we evaluate the *asymptotic convergence* of empirical MCRB and whether it approaches empirical CRB as the number of repeated measurements increases. Second, we evaluate *parameter estimate consistency* through a comparison of the estimates from two equal-sized subsets of the measured data, and assessing the gap between their empirical variances and the theoretical CRB. We also assess the degree of misspecification attributable to incorrect fixed parameters.

While our proposed framework described applies generally to qMRI, we demonstrate its use in arterial spin labeling

(ASL) as an example. ASL is a noninvasive, non-contrast technique that magnetically labels blood water to quantify perfusion: microvascular delivery of blood to exchanging capillaries. The Buxton general kinetic model is the most widely used method for describing the ASL signal and converting measured perfusion-weighted images into quantitative perfusion (mL/min/100g) [8].

2. THEORY

2.1. qMRI Forward Model

Without loss of generality, under prewhitened Gaussian noise and Nyquist sampling, each qMRI voxel is distributed as

$$\mathbf{x}^{(m)} \sim f(\mathbf{x}; \boldsymbol{\theta}, \mathbf{u}) = \mathcal{N}(\mathcal{F}(\boldsymbol{\theta}, \mathbf{u}), \sigma^2 \mathbf{I}_{N \times N}), \quad m = 1, \dots, M, \quad (1)$$

where $\mathbf{x}^{(m)} \in \mathbb{C}^N$ are the measurements from the m^{th} experiment (called dynamics, averages, repetitions, NEX, etc.), $\boldsymbol{\theta} \in \mathbb{R}^P$ are the fixed but unknown physiological parameters, $\mathbf{u} \in \mathbb{R}^N$ are user controllable scanner parameters, \mathcal{F} denotes the discretized signal model evaluated at \mathbf{u} , and σ^2 is the noise variance. When magnitude-only reconstructions are used, the measurements are Rician distributed, but the noise is well approximated as Gaussian when the signal-to-noise ratio (SNR) is sufficiently high [9].

2.1.1. ASL Buxton Model

The Buxton model treats each imaging voxel as a single, well-mixed compartment in which labeled water arrives after an arterial transit time (ATT) with a perfusion rate f , and undergoes longitudinal relaxation characterized by the tissue T_1 . It models the perfusion-weighted signal $\Delta M(t)$ in the following convolutional form [10]:

$$\begin{aligned} \Delta M(t) &= 2\alpha f M_{0b} \int_0^t c(\tau) r(t - \tau) m(t - \tau) d\tau \\ &= 2\alpha f M_{0b} \{c(t) * [r(t) m(t)]\}, \end{aligned} \quad (2)$$

where the factor α accounts for the labeling efficiency and M_{0b} denotes the equilibrium magnetization of arterial blood. The residue and magnetization relaxation functions are

$$r(t) = \exp(-ft/\lambda), \quad m(t) = \exp(-t/T_1), \quad (3)$$

where λ is the blood-tissue partition coefficient. The arterial input function $c(t)$ is modeled as a bolus of duration τ that arrives at time ATT:

$$c(t) = \begin{cases} \exp(-(t - \text{ATT})/T_{1b}), & \text{ATT} < t < \text{ATT} + \tau, \\ 0, & \text{otherwise,} \end{cases} \quad (4)$$

where T_{1b} denotes the blood longitudinal relaxation time.

To fit the general framework of Eq. [1], $\boldsymbol{\theta} = [f, \text{ATT}]^\top$, \mathbf{u} is the vector of sampled time points (called post-labeling delay, PLD), and \mathcal{F} is the Buxton model of Eqs. [2-4].

2.2. Misspecified Cramér–Rao Bounds

Let $p(\mathbf{x})$ denote the true data-generating distribution. When the assumed likelihood $f(\mathbf{x}; \boldsymbol{\theta}, \mathbf{u})$ is correctly specified, the covariance of any unbiased estimator $\hat{\boldsymbol{\theta}}$ is bounded below by the CRB:

$$\mathbf{C}_C = -\mathcal{A}(\boldsymbol{\theta})^{-1}, \quad (5)$$

where $\mathcal{A}(\boldsymbol{\theta})$ is the *expected Hessian* of the log-likelihood,

$$\mathcal{A}(\boldsymbol{\theta}) = \mathbb{E}_p \left[\frac{\partial^2}{\partial \boldsymbol{\theta}^2} \log f(\mathbf{x}; \boldsymbol{\theta}, \mathbf{u}) \right]. \quad (6)$$

However, if $f(\mathbf{x}; \boldsymbol{\theta}, \mathbf{u})$ does not coincide with $p(\mathbf{x})$, the CRB becomes overly optimistic. In this general case, the relevant lower bound is the MCRB, given by [4, 5]

$$\mathbf{C}_M = \mathcal{A}^{-1}(\boldsymbol{\theta}) \mathcal{B}(\boldsymbol{\theta}) \mathcal{A}^{-1}(\boldsymbol{\theta}), \quad (7)$$

where

$$\mathcal{B}(\boldsymbol{\theta}) = \mathbb{E}_p \left[\frac{\partial \log f(\mathbf{x}; \boldsymbol{\theta}, \mathbf{u})}{\partial \boldsymbol{\theta}} \frac{\partial \log f(\mathbf{x}; \boldsymbol{\theta}, \mathbf{u})^\top}{\partial \boldsymbol{\theta}} \right]. \quad (8)$$

When the model is correctly specified, $\mathbf{C}_M = \mathbf{C}_C$. In practice, $p(\mathbf{x})$ is unknown, so we approximate the expectations with empirical estimates $\hat{\mathbf{C}}_M$ and $\hat{\mathbf{C}}_C$, which converge to \mathbf{C}_M and \mathbf{C}_C as $M \rightarrow \infty$ (defined in [1] Eqs. 13-15).

2.3. Evaluation Metrics

We compare $\hat{\mathbf{C}}_M$ and $\hat{\mathbf{C}}_C$ via the congruence transformation

$$\hat{\mathbf{P}} = \hat{\mathbf{C}}_C^{-1/2} \hat{\mathbf{C}}_M \hat{\mathbf{C}}_C^{-1/2} = \mathbf{W}^\top \hat{\mathbf{C}}_M \mathbf{W}, \quad \mathbf{W} \equiv \hat{\mathbf{C}}_C^{-1/2}, \quad (9)$$

where the choice of \mathbf{W} corresponds to whitening with respect to the CRB. If the model is correctly specified, $\hat{\mathbf{P}} \rightarrow \mathbf{I}_{P \times P}$.

The eigenvalues of $\hat{\mathbf{P}}$ quantify the degree of variance amplification when comparing $\hat{\mathbf{C}}_M$ to $\hat{\mathbf{C}}_C$. In particular, the condition number $\kappa \equiv \lambda_{\max}/\lambda_{\min}$ summarizes how anisotropic this amplification is across parameter combinations. Under correct model specification, CRB and MCRB coincide, so that $\lambda_{\max}, \lambda_{\min}, \kappa \rightarrow 1$ as $M \rightarrow \infty$.

3. METHODS

3.1. *in vivo* ASL Scans

Under Institutional Board Approval and informed consent, two healthy volunteers were scanned using pseudo-continuous ASL (pCASL) on a 3T Siemens Vida scanner for the brain and kidney, respectively. Acquisition parameters were: $N = 21$ PLDs (0–1 s step 0.1 s, 1–3 s step 0.2 s), bolus

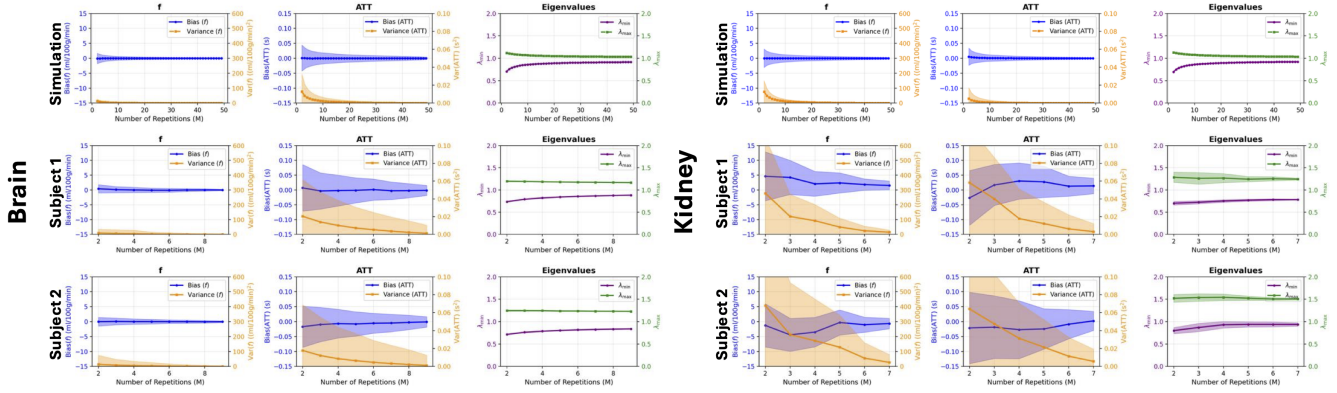


Fig. 1. Simulated and *in vivo* asymptotic convergence as the number of repeated measurements increases. Subject 1 represents the better-conditioned case for both organs. In simulation, as m becomes sufficiently large, all metrics converge to their theoretical values. *In vivo*, the eigenvalues λ_{\max} , λ_{\min} do not converge to 1 as m increases, especially in the kidney.

duration $\tau = 1.5$ s, repeated measurements $M_{\text{total}} = 10$ for the brain, and $M_{\text{total}} = 8$ for the kidney. During kidney imaging, subjects were instructed to maintain a paced breathing pattern to mitigate motion artifacts. A fixed global tissue $T_1 = 1.2$ s for brain and $T_1 = 1.4$ s for kidney was assumed [8]. Scanner-reconstructed magnitude images were used for all subsequent data processing.

3.2. Asymptotic Convergence

To quantify the uncertainty induced by potential misspecification, we compute empirical CRB and MCRB from repeated measurements (see [1] Eqs. 13-15) and examine how they evolve as the number of repetitions increases. We first validate the procedure under a correctly specified setting by simulating the Buxton model for $M_{\text{total}} = 50$ repetitions on 8,000 voxels uniformly spanning physiologically plausible parameter ranges (f range: 0–150 mL/min/100g for the brain, 0–900 mL/min/100g for the kidney; ATT range 0–2 s [8, 11]) and adding Rician noise with variance matched to the *in vivo* scans. For each $M \in \{2, \dots, M_{\text{total}}\}$, we estimate the parameters via MLE, and then compute the bias, variance, λ_{\max} , and λ_{\min} using a bootstrap with $K = 10$ realizations. Each bootstrap resamples the M repetitions (fixed PLDs), refits voxelwise MLE maps, and recomputes the metrics. The same procedure is applied to the *in vivo* datasets. Because ground truth is unavailable, the parameter estimates obtained from all M_{total} repetitions are used as the reference when computing bias. The noise variance is estimated from background regions of the perfusion-weighted images.

3.3. Subset Parameter Estimate Consistency

The ASL datasets are partitioned into two equal-sized subsets with approximately exponential spacing that emphasized either early (Set 1) or late (Set 2) PLDs. For each subset, we

fit parameter maps with MLE, report the magnitude of relative error between the two estimates, and compute empirical parameter variances over $K = 10$ bootstrap realizations for each M . These empirical variances are compared with the theoretical CRB in Eq. [5].

3.4. Fixed Parameter Misspecification

To assess the degree of model misspecification due to fixed-parameter errors, we replace the global tissue T_1 with a tissue-specific T_1 map. Specifically, we assume two perfusion-related tissue types within each organ and assign a distinct T_1 value to voxels in the top 10% of perfusion-weighted signal intensity. All acquisition parameters, PLDs, and estimation procedures are kept identical. We then compare the resulting λ_{\max} , λ_{\min} , and κ against the global T_1 baseline.

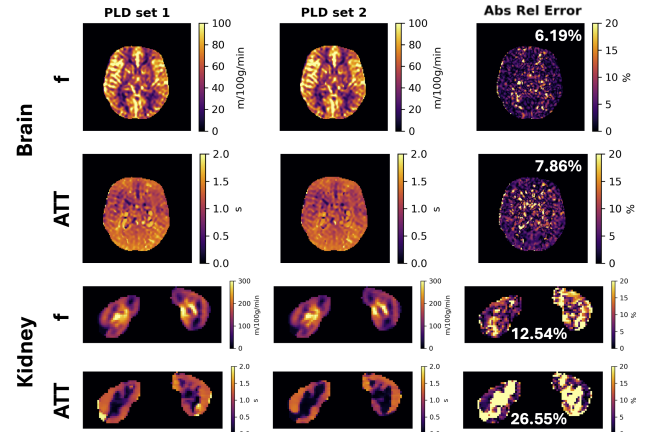


Fig. 2. Parameter estimates from two PLD subsets and their average relative error over all voxels (white text). Errors in the kidney are larger and more spatially heterogeneous.

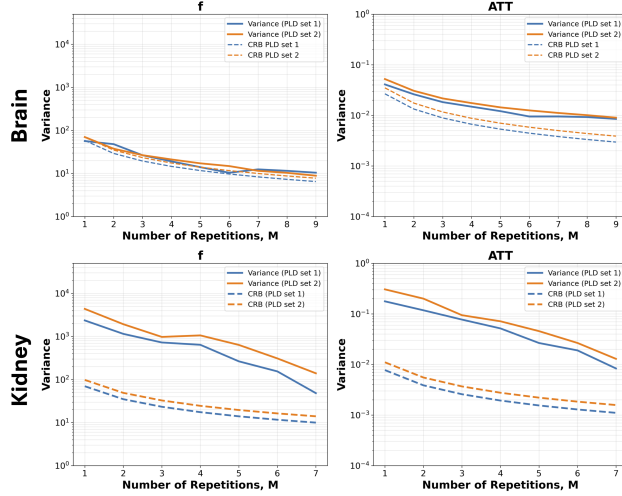


Fig. 3. Empirical MLE variance compared with the theoretical CRB (dotted lines). In the brain, the variance of f remains tightly bounded by the CRB, and ATT shows a similar but slightly looser bound. In contrast, in the kidney the empirical variance exceeds the CRB by a larger margin, indicating that the CRB underestimates the estimation uncertainty.

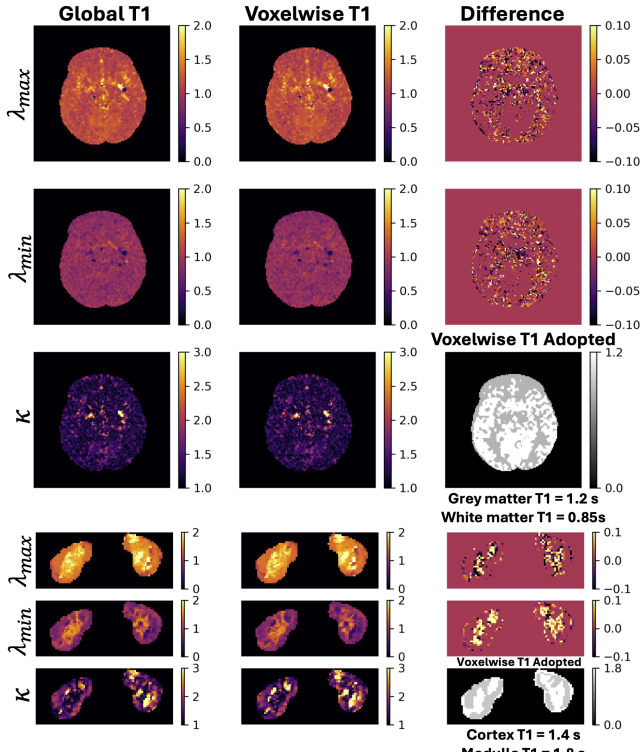


Fig. 4. Eigenvalues and condition number obtained with a global T_1 (left), a voxelwise T_1 (middle), and their difference (right). Voxelwise T_1 lowers both eigenvalues, yet the condition number remains large, suggesting that fixed T_1 and model mismatch both contribute to misspecification.

4. RESULTS

Fig. 1 summarizes the simulated and *in vivo* asymptotic convergence. In simulation, as the number of repetitions increases, both bias and variance decay toward 0, and the eigenvalues approach 1 from above and below. For the *in vivo* data, the gap between λ_{\max} and λ_{\min} plateaus at values larger than simulation predicts. Fig. 2 shows the subset estimate consistency results. Relative errors in the kidney are larger and exhibit greater spatial heterogeneity. Fig. 3 compares empirical variances with the theoretical CRB on a logarithmic scale. In the kidney, the empirical variance deviates from the CRB and is much less tightly bounded. Fig. 4 examines fixed parameter misspecification by replacing the global tissue T_1 with voxelwise values. Although both eigenvalues decrease with voxelwise T_1 , the large condition number indicates that misspecification arises from both the fixed T_1 assumption and the underlying model.

5. DISCUSSION AND CONCLUSION

This study presents a general framework for evaluating model misspecification in quantitative MRI. We assess misspecification through two criteria: the asymptotic convergence of variance bounds, and the consistency of parameter estimates. We also isolate model errors from fixed parameter misspecification. Using the ASL Buxton model as an case, our results suggest that the Buxton model appears to be specified in the brain, but may be moderately misspecified in the kidney. Future work will expand validation to larger cohorts and organs, and enable model selection across candidate qMRI models.

Many investigators have questioned the accuracy of the Buxton model assumptions in accurately capturing quantitative perfusion, particularly in the presence of disease. This work provides a data driven approach of assessing the validity of the model's assumptions, even in the absence of ground truth measurements [12, 13].

One plausible explanation for the Buxton model's misspecification in the kidney is because it assumes that labeled blood entering a voxel does not flow out and undergoes an exponential T_1 decay. In the kidney, however, labeled blood can exit the imaging voxel via efferent arterioles. This unmodeled outflow accelerates signal decay at long PLDs and leads to systematic underestimation of perfusion, as reported in [14]. Partial-volume effects may also contribute to misspecification, as each ASL voxel often contains a mixture of compartments with distinct perfusion properties [15]. We also find that using a fixed global tissue T_1 introduces additional error. Prior work [16] has shown that jointly estimating T_1 in ASL compromises perfusion accuracy. Therefore, an additional T_1 mapping acquisition is recommended if feasible.

Our approach provides a global metric for model misspecification based on the condition number of \hat{P} . Other discrepancy measures such as the matrix trace and KL divergence

could also be used. Our work is also closely related to the information matrix and Hausman test proposed in [4]. While we focused on global measures, these tests could be applied per-voxel, though spatial correlations and multiple-comparison testing would need to be taken into account.

6. COMPLIANCE WITH ETHICAL STANDARDS

All data in this study were acquired under institutional review board (IRB) approval and informed consent.

7. ACKNOWLEDGEMENTS

This work is supported by NSF CCF-2239687 (CAREER) and the terminated NIH grant R01-EB033916.

8. REFERENCES

- [1] Stefano Fortunati, Fulvio Gini, Maria S Greco, and Christ D Richmond, “Performance bounds for parameter estimation under misspecified models: Fundamental findings and applications,” *IEEE Signal Processing Magazine*, vol. 34, no. 6, pp. 142–157, 2017.
- [2] Ji Meng Loh, Martin A Lindquist, and Tor D Wager, “Residual analysis for detecting mis-modeling in fmri,” *Statistica Sinica*, pp. 1421–1448, 2008.
- [3] Laura M. Parkes and Paul S. Tofts, “Improved accuracy of human cerebral blood perfusion measurements using arterial spin labeling: accounting for capillary water permeability,” *Magnetic Resonance in Medicine*, vol. 48, no. 1, pp. 27–41, 2002.
- [4] Halbert White, “Maximum likelihood estimation of misspecified models,” *Econometrica: Journal of the Econometric Society*, pp. 1–25, 1982.
- [5] Quang H. Vuong, “Cramér-rao bounds for misspecified models,” Tech. Rep., Social Science Working Paper 652, California Institute of Technology, 1986.
- [6] Simone Cerreia-Vioglio, Lars Peter Hansen, Fabio Maccheroni, and Massimo Marinacci, “Making decisions under model misspecification,” *Review of Economic Studies*, p. rda046, 2025.
- [7] Karim Abed-Meraim, Nguyen Linh Trung, et al., “Misspecified cramer-rao bounds for blind channel estimation under channel order misspecification,” *IEEE Transactions on Signal Processing*, vol. 69, pp. 5372–5385, 2021.
- [8] David C Alsop, John A Detre, Xavier Golay, Matthias Günther, Jeroen Hendrikse, Luis Hernandez-Garcia, Hanzhang Lu, Bradley J MacIntosh, Laura M Parkes, Marion Smits, et al., “Recommended implementation of arterial spin-labeled perfusion mri for clinical applications: a consensus of the ismrm perfusion study group and the european consortium for asl in dementia,” *Magnetic resonance in medicine*, vol. 73, no. 1, pp. 102–116, 2015.
- [9] Hákon Gudbjartsson and Samuel Patz, “The rician distribution of noisy mri data,” *Magnetic resonance in medicine*, vol. 34, no. 6, pp. 910–914, 1995.
- [10] Richard B. Buxton, Lawrence R. Frank, Eric C. Wong, Bettina Siewert, Steven Warach, and Robert R. Edelman, “A general kinetic model for quantitative perfusion imaging with arterial spin labeling,” *Magnetic Resonance in Medicine*, vol. 40, no. 3, pp. 383–396, 1998.
- [11] Aghogho Odudu, Fabio Nery, Anita A Harteveld, Roger G Evans, Douglas Pendse, Charlotte E Buchanan, Susan T Francis, and María A Fernández-Seara, “Arterial spin labelling mri to measure renal perfusion: a systematic review and statement paper,” *Nephrology Dialysis Transplantation*, vol. 33, no. suppl_2, pp. ii15–ii21, 2018.
- [12] Audrey P Fan, Jia Guo, Mohammad M Khalighi, Praveen K Gulaka, Bin Shen, Jun Hyung Park, Harsh Gandhi, Dawn Holley, Omar Rutledge, Prachi Singh, et al., “Long-delay arterial spin labeling provides more accurate cerebral blood flow measurements in moyamoya patients: a simultaneous positron emission tomography/mri study,” *Stroke*, vol. 48, no. 9, pp. 2441–2449, 2017.
- [13] Adam Bush, Yaqiong Chai, So Young Choi, Lena Vavavu, Scott Holland, Aart Nederveen, Thomas Coates, and John Wood, “Pseudo continuous arterial spin labeling quantification in anemic subjects with hyperemic cerebral blood flow,” *Magnetic resonance imaging*, vol. 47, pp. 137–146, 2018.
- [14] Bandar A. Alhummiany, Daniel Shelley, Mark Saysell, Maria A. Olaru, Benjamin Kühn, Daniel L. Buckley, Jon Bailey, Keith Wroe, Carol Coupland, Michael W. Mansfield, and Steven P. Sourbron, “Bias and precision in magnetic resonance imaging-based estimates of renal blood flow: Assessment by triangulation,” *Journal of Magnetic Resonance Imaging*, vol. 55, no. 4, pp. 1241–1250, 2022.
- [15] Michael A Chappell, Flora A Kennedy McConnell, Xavier Golay, Matthias Günther, Juan A Hernandez-Tamames, Matthias J van Osch, and Iris Asllani, “Partial volume correction in arterial spin labeling perfusion mri: A method to disentangle anatomy from physiology or an analysis step too far?,” *Neuroimage*, vol. 238, pp. 118236, 2021.

[16] Peter Bladt, Arnold J. den Dekker, Philippe Clement, Eric Achten, and Jan Sijbers, “The costs and benefits of estimating t_1 of tissue alongside cerebral blood flow and arterial transit time in pseudo-continuous arterial spin labeling,” *NMR in Biomedicine*, vol. 33, no. 12, pp. e4182, 2020.